Nuclear Instruments and Methods in Physics Research B 360 (2015) 103–110

Contents lists available at ScienceDirect

Nuclear Instruments and Methods in Physics Research B

journal homepage: www.elsevier.com/locate/nimb

Band structure effects in the energy loss of low-energy protons and deuterons in thin films of Pt

C.E. Celedón [a,b,*], E.A. Sánchez [a], L. Salazar Alarcón [a], J. Guimpel [a], A. Cortés [b], P. Vargas [b], N.R. Arista [a]

[a] Centro Atómico Bariloche and Instituto Balseiro, San Carlos de Bariloche, Argentina
[b] Laboratorio de Colisiones Atómicas, Departamento de Física, UTFSM, Valparaíso, Chile

ARTICLE INFO

Article history:
Received 4 April 2015
Received in revised form 11 August 2015
Accepted 11 August 2015
Available online 28 August 2015

Keywords:
Stopping power
Pt
Band structure

ABSTRACT

We have investigated experimentally and by computer simulations the energy-loss and angular distribution of low energy ($E < 10$ keV) protons and deuterons transmitted through thin polycrystalline platinum films. The experimental results show significant deviations from the expected velocity dependence of the stopping power in the range of very low energies with respect to the predictions of the Density Functional Theory for a jellium model. This behavior is similar to those observed in other transition metals such as Cu, Ag and Au, but different from the linear dependence recently observed in another transition metal, Pd, which belongs to the same Group of Pt in the Periodic Table. These differences are analyzed in term of the properties of the electronic bands corresponding to Pt and Pd, represented in terms of the corresponding density of states. The present experiments include also a detailed study of the angular dependence of the energy loss and the angular distributions of transmitted protons and deuterons. The results are compared with computer simulations based on the Monte Carlo method and with a theoretical model that evaluates the contributions of elastic collisions, path length effects in the inelastic energy losses, and the effects of the foil roughness. The results of the analysis obtained from these various approaches provide a consistent and comprehensive description of the experimental findings.

1. Introduction

The physics of the energy loss of light ions in solids is a subject of great interest for numerous areas of basic and applied research. Unlike the high-energy range, where experimental stopping power data is available for many materials, experimental work on low-energy hydrogen beams is rather scarce. For this reason, several important aspects of the interaction process are currently the subject of theoretical and experimental investigation. In particular, the interaction of light ions such as protons, deuterons and He ions with metals and insulators has revealed new and unexpected aspects of the interaction process, and so this area has become a very attractive field of low-energy research.

Platinum, as a film, nanoparticle or nano-composite has been widely used in different applications in the last decade, such as functionalization of nanostructures for fuel cell electrodes [1], biological sensors [2], catalyzer for oxygen reduction [3], improvements of signals in Raman spectroscopy (SERS) [4], anticancer agent [5], and improvement in the efficiency of proton therapy [6], where its topological (roughness, inhomogeneities) and physical characteristics (crystallinity, electronegativity) may become a relevant factor for the functionalization of organic or inorganic species, or may affect the charge or energy transfer in the interaction with electromagnetic or ionizing radiation.

One of the most conspicuous aspects of the electronic energy loss of light ions at low energies in metallic targets is the observed deviations from the expected velocity dependence in the case of noble metals. The standard theories of the energy loss of slow ions in metals, which consider the target as a simple free electron gas, predict a proportionality of the stopping power with the ion velocity [7–11]. This velocity dependence was experimentally confirmed for most metallic targets. However a distinct behavior of the low-energy stopping coefficient was observed by Valdés et al. [12,13] for some metals containing *d* electrons, such as Cu, Ag, and Au. This effect was theoretically explained by the existence of a minimum energy transfer for the excitation of *d* electrons, due to a shift in the corresponding density of states (DOS) of those metals with respect to the Fermi energy (a so-called "threshold effect"). This effect was studied in more detail in recent experiments performed at two laboratories [14–16]. Moreover, the theoretical explanation of the origin of the effect was confirmed by

* Corresponding author at: Laboratorio de Colisiones Atómicas, Departamento de Física, UTFSM, Valparaíso, Chile.

http://dx.doi.org/10.1016/j.nimb.2015.08.018
0168-583X/

more sophisticated calculations using Time Dependent Density Functional Theory (TD-DFT) [17].

On the other hand, in recent experiments with Pd foils [18], we have found no deviations from the velocity proportionality. This behavior was reproduced by modeling the Pd *d* electrons as a free electron gas with $r_s = 1.51$ [18,19], but there are so far no *ab initio* calculations that could provide a more complete theoretical treatment of this case. Further evidences on the role of *d* electrons in the energy loss of light ions in metals have been given recently by Goebl et al. [20]. In particular, they obtained new results for the energy loss of protons and deuterons in Pt. The data for velocities below 0.4 a.u. show some indications of possible deviation from the velocity proportionality, although the reported effect is of the order of one standard deviation. Therefore, no conclusive evidences on this effects could so far be obtained in the case of Pt. Hence, from the results of these experiments it stems that new experimental results for the low-energy stopping power of protons and deuterons in Pt is required in order to provide more evidences on the existence or not of deviations from the velocity proportionality in this transition metal. This is a question of considerable interest for a complete understanding of the energy loss process in the range of very low energies, with also important consequences for the theoretical efforts to explain the energy loss mechanism in a systematic way. In this work we measured the energy loss of protons and deuterons in Pt foils, in the range of 1–10 keV, with the purpose to provide new results that help to clarify the mentioned behavior and to obtain further evidences of the influence of band-structure effects in the low-energy range. The experimental results presented here include detailed studies of the velocity dependence, angular distributions of transmitted ions and angular dependence of the energy loss. The results are analysed through simulations and theoretical predictions based on DFT and alternative models, and considering realistic density of states of Pt obtained from tight binding linear muffin tin orbital (TB-LMTO) calculations.

2. Experimental method

The experiments were performed in the Low Energy Accelerator (LEA) laboratory of the Centro Atómico Bariloche, Argentina (LEA/CAB).

The energy loss measurements with proton and deuteron beams were performed on Pt polycrystalline self-supported foils mounted on transmission electron microscopy (TEM) grid supports, using the transmission geometry as described in a previous work [18]. In this geometry, the beam with incident energy E_0 traverses the thin foil placed perpendicular to the incident beam direction, and the energy spectra of the transmitted ions is measured in the forward direction, close to the outgoing surface normal. The energy lost by a projectile is determined as the difference between the incident energy E_0 and the most probable exit energy E_p obtained from the spectrum of the transmitted ions. The stopping power can be directly obtained by dividing the energy loss $(E_0 - E_p)$ by the foil thickness, and the stopping cross section (SCS) by dividing the stopping power by the atomic target density. The use of this geometry, minimizes the contributions to the energy loss due to the elastic collisions with target nuclei and to the path enlargement produced by multiple scattering events, maximizing the contribution due to the electron interaction (electronic stopping power).

The H^+, H_2^+, D^+ and D_2^+ beams were produced by a Colutron BK series hot-cathode ion source [22]. The ion beam was accelerated, focused and selected in mass and charge by a Wien filter; and then deflected 18° to remove the neutral particles before entering into a high vacuum collision chamber. The energy spectra (energy loss distributions) of projectiles that traversed the Pt foils were measured using a 127° electrostatic cylindrical energy analyzer with an energy and angular resolution of 2% (FWHM) and 1.5°, respectively.

The acquired energy spectra were corrected by the transmission function of the analyzer that is proportional to the analyzed energy, and by the efficiency of the electron multiplier (ETP AEM 1000), that under present experimental conditions, presents a linear dependence with the analyzed energy [23]. Additionally, the dependence of the ion fraction with the outgoing projectile energy was also taken into account. Since the charge fraction of an outgoing projectile that traverse a foil depends on the outgoing surface conditions, we used for the correction function a curve fitted from the experimental values reported in references [24–26] measured for carbon samples. This was done with these experimental values because we detected a very thin layer of carbon on the foil surfaces as it will be discussed in the next section. By considering these three dependences, a total correction function that accounts for the variation of the total efficiency as function of the detection energy can be obtained. This function is presented in the left upper panel of Fig. 1 together with the contributions from the analyzer transmission, the detection efficiency and the outgoing ion fraction, all of them normalized to 1 at 10 keV for comparison. The corrected spectra were obtained by dividing the acquired spectra by the total correction function.

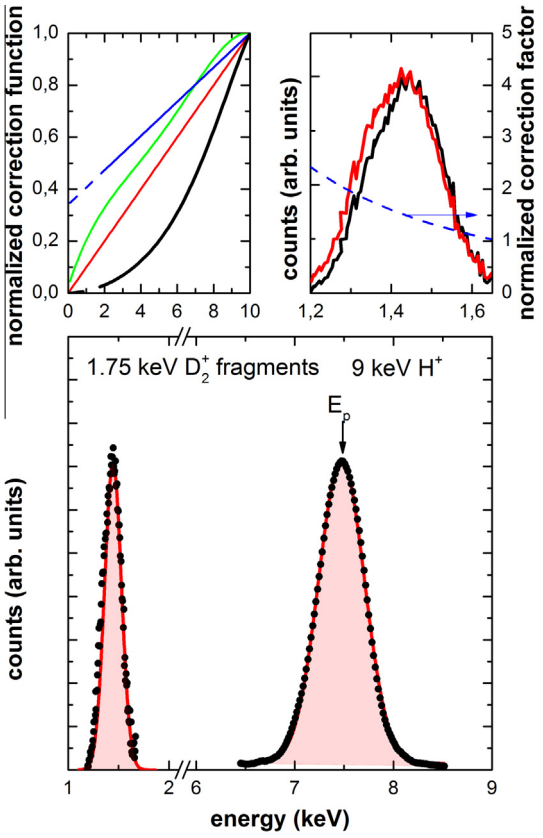

Fig. 1. Left upper panel: Energy dependence of the correction functions due to the analyzer transmission (red), the detector efficiency (blue), and the outgoing ion fraction (green); together with the total correction function (thick black). All of them were normalized to 1 at 10 keV for comparison. Right upper panel:Energy spectra of 1.75 D_2^+ fragments transmitted through a 15 nm Pt film. The Black line corresponds to the uncorrected spectrum, and the red one to the spectrum corrected by multiplying the uncorrected one by the normalized correction factor (dash blue). See text for correction factor definition. Lower panel: Energy spectra of 1.75 D_1^+ fragments and 9 keV protons transmitted through a 15 nm Pt film (black solid circles). Red solid line and light red area correspond to function shape and area of gaussian fit. (For interpretation of the references to color in this figure legend, the reader is referred to the web version of this article.)

In the right upper panel of Fig. 1 we show the experimental results obtained for 1.75 keV D^+ transmitted through a 15 nm Pt selfsupported film, together with the corresponding corrected energy spectrum. The spectra were normalized in height to 1 for comparison. In this panel we also show with dashed lines, the normalized correction factor, i.e. the inverse of the correction function, that multiplies the acquired spectrum. In this panel the correction factor was normalized to 1 for the higher ion energies. This produces an increase of the low energy tails by a factor of 2, shifting the energy distribution to lower energies. In the range of our experimental measurements, the shift values of the most probable exit energy E_p are less than 15 ± 5 eV, being the error in the energy loss determination of about of 1% for the higher projectile energy and about 3% for the lower ones.

In the lower panel of Fig. 1 we present spectra of the transmitted D_2^+ fragments ($E_0 = 1.75$ keV) and hydrogen ions ($E_0 = 9$ keV) after interacting with a 15 nm Pt foil. The most probable exit energy (E_p) of the spectra were obtained by fitting the experimental results with Gaussian distribution functions. The most probable exit energy agrees with the mean value within 1%. As shown in the figure, one obtains for higher energies an excellent fitting using a Gaussian distribution function. The symmetry of the spectrum in this energy range is a characteristic of the transmission method and, is the basis for accurate determinations of ion energy losses in thin foils [27]. At lower energies (D_2^+ fragments), the distribution shows an increase of the low-energy tail of the spectrum corresponding to higher electronic energy losses produced by pathlength increases due to the multiple scattering of the beam particles in the medium. In this case the fitting with a gaussian distribution is performed considering the region around the maximum and the high-energy side of the experimental distribution. In this way, the effects of pathlength increase in the reported stopping power values are eliminated. With this method the error in the E_p determination is of the order of 3%. This value is in good agreement with the Monte Carlo result, excluding the projectile with a enlargement path length due to elastic collision.

2.1. Foil targets

The samples used for the energy loss measurements were produced by deposition of Pt by the sputtering method on cleaved polished NaCl rock salts. After a careful dissolution of the salt at 49°C , the foils floating on the surface of the deionized water were transferred to TEM grids. The films were deposited simultaneously onto NaCl and very flat SiO_2 and glass substrates. The later were used to determine the film thickness and the bulk density by low angle X-ray reflectometry (XRR), and the film composition by X-ray Photoelectron Spectroscopy (XPS). In this way several films were produced, with thicknesses in the range of 15–16 nm. Fig. 2 shows the low angle reflected intensity oscillations from two samples of Pt. These oscillations are due to the interference between the X-rays reflected at the vacuum-film and film-substrate interfaces. At the low angle region, the refractive index cannot be neglected. It can be expressed as $n = 1 - \delta$, with $\delta \ll 1$ and proportional to the electronic density of the material. Since the electronic density of glass is smaller than that of Pt, there is a π phase change on reflection at the film-substrate interface. Taking into account these effects, the peak positions in the reflected intensity are expressed by

$$sin^2\theta_m = \left(m + \frac{1}{2}\right)^2 \left(\frac{\lambda}{2t}\right)^2 + \theta_c^2 \quad (1)$$

where θ_m is the position of the mth order maximum, $m = 0, 1, 2, \ldots, \infty$, λ is the X-ray wavelength (0.15418 nm for Cu-K_α radiation), t is the film thickness, and $\theta_c = \sqrt{2\delta}$ is the critical angle for total reflection at the vacuum-film interface. By fitting the relation $sin^2\theta_m$ vs $(m + 1/2)^2$ with a linear regression one obtain the thickness of the film. Another method to get the thickness and density values is by adjusting the experimental data using the Parratt formalism [28–30]. In Fig. 2 we present the X-ray intensity measured as a function of the deviation angle for two samples, together with the fittings done with the Parratt formalism. In the inset of Fig. 2, the position of the peaks as a function of the mth order (as presented in Eq. (1)) is also shown. Both methods gave similar thickness values (15.0 and 15.7 nm for this two samples) and densities within ±2% of the bulk density of Pt Ref. [31].

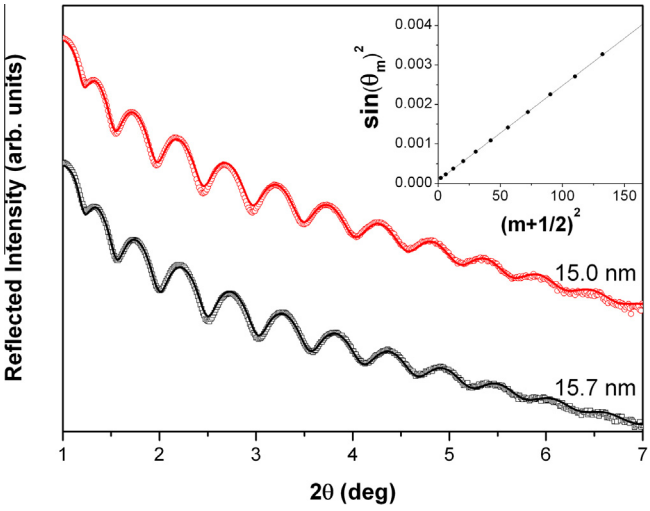

Fig. 2. Low angle reflected X-ray intensity as a function of deviation angle from two different Pt samples grown on a glass substrate (Red open circles and Black open squares). The solid lines show fits to the data points using the Parratt formalism for the reflectivity Ref. [29]; and the inset, the angle for maximum intensity θ_m as a function of the peak order m obtained from the data presented in black. The thickness values obtained with both methods for the red and black data are 15.0 and 15.7 nm, respectively. The density values obtained with the Parratt formalism agree with the bulk density of Pt within ±2%. (For interpretation of the references to color in this figure legend, the reader is referred to the web version of this article.)

The way the scattered intensity and higher order peaks vanish for higher angles indicate a film roughness (or thickness uncertainty) of about 8%. The value obtained for the film surface roughness performed by an Atomic Force Microscope (AFM) was about 15%.

Possible contamination produced by handling the sample in air, from the thin film deposition chamber to the high vacuum collision chamber were evaluated by performing a depth profiling of a Pt film deposited on a flat SiO_2 substrate by X-ray photoelectron spectroscopy (XPS). The results indicate that the film is pure, with traces of C and O impurities located just at the surface, with C the dominant impurity (about 70%). An evaluation of the presence of this contamination on the film surfaces performed by SRIM simulations [32] gives uncertainties in the stopping power of the order of 5%.

By taking into account all the uncertainties before mentioned, we estimate that the total uncertainties in the stopping power determination varies from about ±15% for the lowest ion energies to ±10% for the higher ones.

3. Monte Carlo simulations

The method and characteristics of the Monte Carlo (MC) simulations were similar to those applied in previous works [18,33,34]. These simulations included information on the target properties, surface roughness, stopping forces, intrinsic straggling and inter-

atomic potential, in order to analyze and explain the main features of the experiments. The interatomic potential used was a Molière type, with screening radius determined from the analysis of the multiple scattering distributions (see Section 5.1). The binning energy used by the MC simulations of energy loss spectra was 10 eV. The projectile energy range used in the MC simulations was the same as in the experimental determinations. The surface roughness was modeled using a Gaussian distribution and the roughness-coefficient value was obtained from the energy-angle dependence of the energy loss as described below. The input values of the electronic stopping forces required by the MC simulations were obtained by adjusting the results of the most probable energy loss obtained from these simulations with the corresponding experimental values determined from the energy distributions.

4. Three components model

The angular dependence of the mean energy loss of ions transmitted through a thin film, with the observation angle θ, can be described with the so-called three-components model (TCM) of Ref. [34], which consists of three contributions:

1. *Changes in the electronic energy loss due to path length increase.* This contribution is given by

$$\Delta E_{elec}(\theta) - \Delta E_{elec}(0) = \frac{1}{2}\left(\frac{1}{\cos(\theta)} - 1\right)\Delta E_{elec}(0); \quad (2)$$

2. *Elastic energy loss.* This effect is modeled considering the elastic energy transfer in collisions with target atoms given by

$$\Delta E_{nucl}(\theta) \simeq 4\frac{M_1 M_2}{(M_1+M_2)^2} E \sin^2(\theta/2); \quad (3)$$

where E is the mean ion energy and M_1 and M_2 are the ion and target masses.
and
3. *The effect of the foil roughness.* This effect is given by

$$\Delta E(\theta)_{rough} - \Delta E(0)_{rough} = \rho^2\,\overline{\Delta E}\left(\frac{\partial \ln|F_{MS}(\theta,\Delta x)|}{\partial \ln \Delta x} - \frac{\partial \ln|F_{MS}(0,\Delta x)|}{\partial \ln \Delta x}\right) \quad (4)$$

where F_{MS} is the multiple scattering function [35], ρ is the usual roughness coefficient, defined as the variance of the foil thickness distribution relative to its mean thickness value Δx, and $\overline{\Delta E}$ is the mean energy loss in the foil.

More details about this theoretical model can be found in Ref. [34].

5. Experimental results

5.1. Angular distributions and energy losses

Fig. 3 shows a 3D representation of the complete set of measurements performed using an incident beam of protons with energy of 9 keV, after transmission through a Pt foil of thickness of 15 nm. The figure shows the spectra of transmitted protons at various angles of emergence between 0 and 20 degrees. The projected values on the plane to the left are the areas of each distribution (normalized to the value at zero angle). This projection yields the multiple scattering angular distribution of transmitted particles.

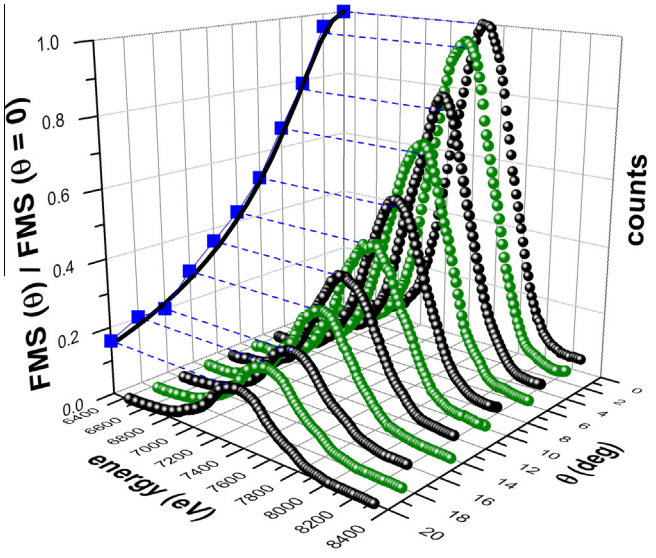

Fig. 3. Energy spectra of protons with incident energy $E_0 = 9$ keV transmitted through a thin film of Pt (15 nm), for different exit angles (θ = 0–20°). Circles show the experimental energy spectrum for each observation angle while solid squares show the normalized angular distribution obtained from the areas of each energy spectra.

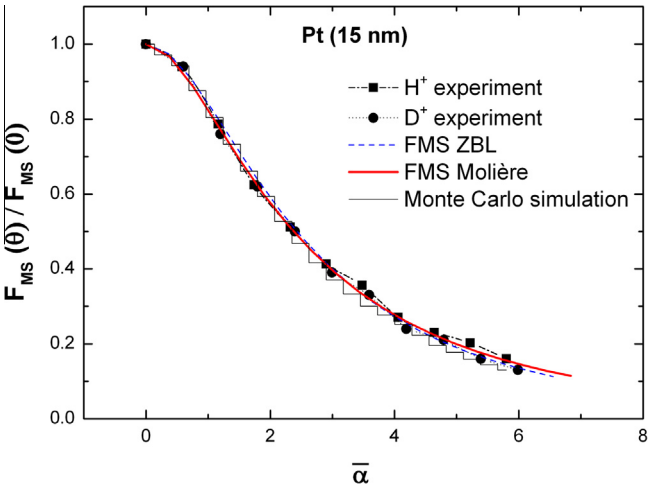

Fig. 4. Normalized angular distribution of 9 keV protons and deuterons transmitted through a thin film (15 nm) of Pt in terms of the reduced angle $\alpha = (Ea/2Z_1Z_2e^2)\theta$.

The results of similar experiments using proton and deuteron beams are shown in Fig. 4, which shows the angular distributions as a function of the reduced angle $\alpha = (Ea/2Z_1Z_2e^2)\theta$, given by the multiple scattering (MS) theory [35], where E is the mean ion energy, a is the screening length, and Z_1 and Z_2 are the ion and target atomic numbers. The figure shows the experimental results, the calculations using the model potentials, and the results of the MC simulations. The excellent scaling of the experimental points for both isotopes is in agreement with the scaling prediction of the angular distributions given by the MS theory. The experimental normalized angular distributions (AD) were used to determine the most appropriate interatomic potential that describes the whole set of experimental results. The procedure consists of fitting the AD according to the standard MS formulation [35], considering two alternative models for the interaction potential: Molière and ZBL potentials [36,37]. The value of the roughness coefficient was obtained using the Three-Components Model (TCM) [38] to reproduce the angular dependence of the energy loss as described in

Refs. [38–40]. The theoretical calculations of the AD of transmitted particles are shown by the lines in Fig. 4, for the Molière and the ZBL potentials with screening lengths $0.83a_L$, $0.63a_L$ respectively, being a_L the Lindhard screening length [36,37]. Additional calculations and simulations using the Lenz-Jensen and power-law potentials were also performed, but they did not agree so well with the experiments in this low-energy range.

Figs. 5 and 6 show the angular dependence of the energy loss for protons and deuterons respectively. The lines in these figures show the theoretical calculation performed using the TCM and the Monte Carlo simulations (MC) described before. The foil roughness value obtained from the analytical adjustment of the experimental energy-angle distributions for this foil was 12%, in reasonable agreement with the values obtained by low angle X-ray reflectometry (8%) and AFM (15%) measurements. We notice the very good agreement obtained in both cases with the TCM and MC methods; we also notice the utility of the TCM in order to separate the contributions of path-length enlargement, foil roughness effects and elastic energy loss terms. The MC simulations yield also useful information on the contribution of nuclear energy losses, which in the present case (light ions on heavy target elements, and transmission method) is very small. Thus, for instance, from the MC simulations we obtain a ratio of nuclear to electronic energy loss of 0.5% in the case of protons measured at zero angle, and 0.9% for $\theta = 20°$. The corresponding values of nuclear energy losses for deuterons are nearly twice those for protons with the same energy, and so also very small. It should be noted that the total (electronic plus nuclear) energy loss at zero angle for the case shown in Fig. 5 is 1465 eV. Similar analysis were performed for various energies in order to check the contribution of nuclear energy losses. For the conditions of our experiments, i.e., in transmission measurements at zero angle and with small angular resolution, the MC simulations for protons in the velocity interval of 0.6–0.3 a.u. yield an elastic energy loss contribution of 0.5–1%, while for velocities between 0.3 and 0.2 a.u. it increases from 1% to 2%. Therefore, the lowest-energy measurements in forward direction (to be analyzed below) include an estimated elastic contribution of *ca.* 4% in the case of deuterons, which is too small to affect the velocity dependence of the forward energy loss.

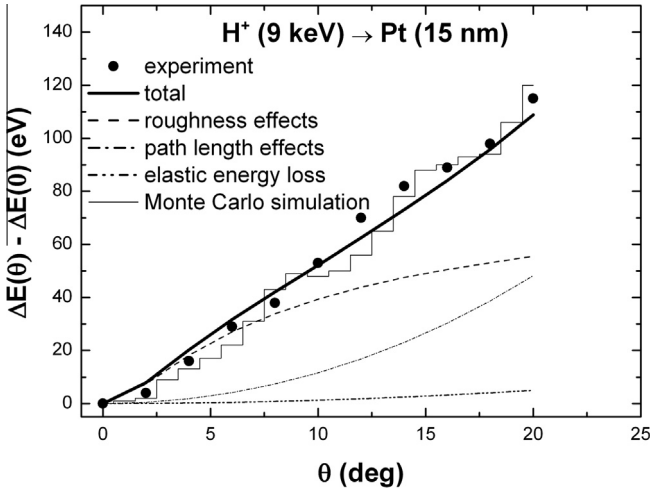

Fig. 5. Angular dependence of the energy loss of 9 keV protons transmitted through a polycrystalline Pt film of 15 nm (referred to the energy loss in the forward direction). Dotted line: effects of foil roughness. Dashed line: contribution of path-length enlargement. Dash-dotted line: contribution of elastic scattering.

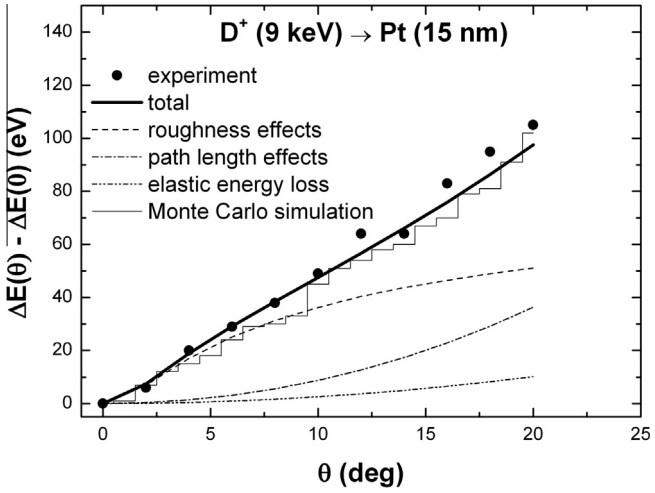

Fig. 6. Angular dependence of the energy loss of 9 keV deuterons transmitted through a polycrystalline Pt film of 15 nm (referred to the energy loss in the forward direction). Dotted line: effects of foil roughness. Dashed line: contribution of path-length enlargement. Dash-dotted line: contribution of elastic scattering.

5.2. Velocity dependence

The experimental results obtained for several samples of different thickness for the stopping power and the corresponding stopping cross section of H^+, D^+, and those of protons and deuterons, obtained from the fragmentation of incident H_2^+ and D_2^+, are shown in Figs. 7 and 8. To obtain the values of the stopping power we divided the experimental energy loss by the film thickness, and to obtain the SCS we used the atomic density of Pt, both obtained from the XRR analysis.

With the aim to compare the present results with previous experimental data, we present in Fig. 7 the SCS as a function of the ion velocity as reported in references [20,21], together with our experimental results obtained as a function of the mean ion velocity ($v = (v_0 + v_p)/2$). These results are in very good agreement, showing consistency between the different methods used to evaluate the scattering cross section. We have also included

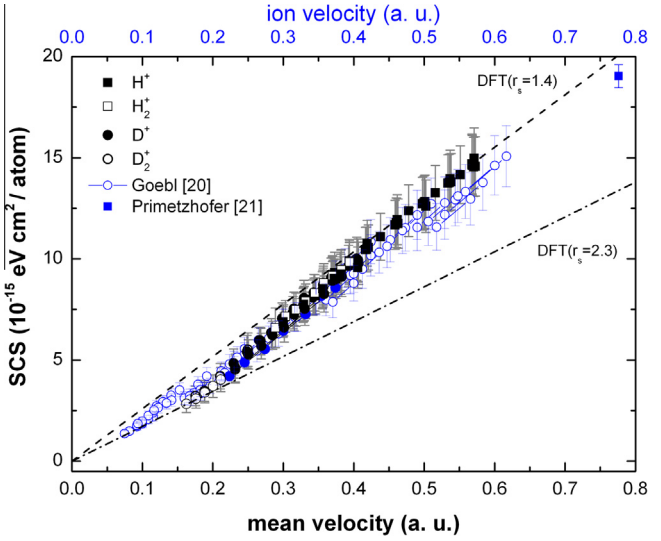

Fig. 7. Stopping cross section for hydrogen ions in Pt, as a function of the mean projectile velocity (lower scale). Solid squares, open squares, solid circles and open circle symbols show proton, molecular-proton-fragments, deuterons and molecular-deuteron-fragments data respectively. Blue-circles and blue-squares symbols are previous SCS data as a function of the ion velocity (upper scale) as reported in Ref. [20] and [21], respectively. The dash and dash-dot lines correspond to DFT calculations for a free-electron gas with $r_s = 1.4$ and $r_s = 2.3$. (For interpretation of the references to color in this figure legend, the reader is referred to the web version of this article.)

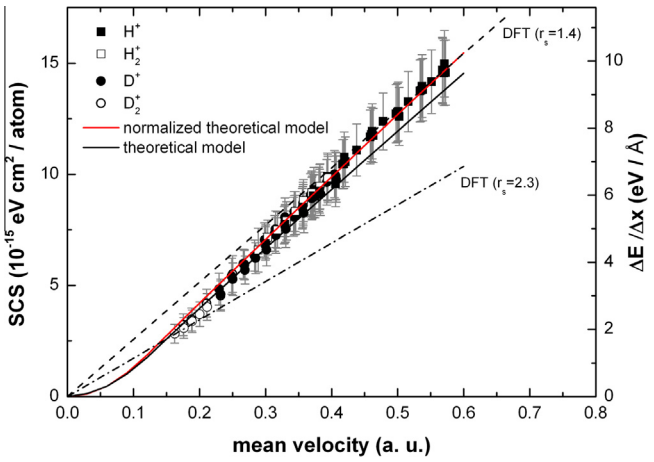

Fig. 8. Stopping cross section for hydrogen ions in Pt, as a function of the mean projectile velocity (lower scale). The scale on the right side shows the energy loss values $\langle \frac{dE}{dx} \rangle$. The solid and open squares and circles show the current measurements. The solid red line shows the SCS values obtained with the theoretical model of Eq. (5), normalized to the mean value of the highest experimental SCS data value. The solid black line correspond to the absolute values given by Eq. (5). The dash and dash-dot lines show the DFT calculations for a free-electron gas with $r_s = 1.4$ and $r_s = 2.3$, respectively. (For interpretation of the references to color in this figure legend, the reader is referred to the web version of this article.)

two straight lines in the figure that correspond to the theoretical DFT predictions for a jellium model of the metal [11], considering two values of the Wigner–Seitz radius r_s of 2.3 and 1.4. These r_s values correspond to 2 and 9 electrons per Pt atom respectively.

In Fig. 8, we present our experimental results, together with the theoretical results obtained with a simple jellium model as explained in Fig. 7, and with those obtained with the model proposed in the next section. In this figure the axis corresponding to the Stopping Cross Section and to the stopping power are shown. This set of data shows a clear deviation of the experimental stopping power values from the DFT predictions in the low energy range, but are very well reproduced by the proposed model (see comments in the next section). In order to see more clearly the deviation from the v-proportionality we show in Fig. 9 the friction coefficient Q defined by the ratio $Q = \frac{1}{v}\langle \frac{dE}{dx} \rangle$. A very clear departure from the DFT prediction is here observed for $v < 0.4$. A detailed analysis of this effect is made in the following Section.

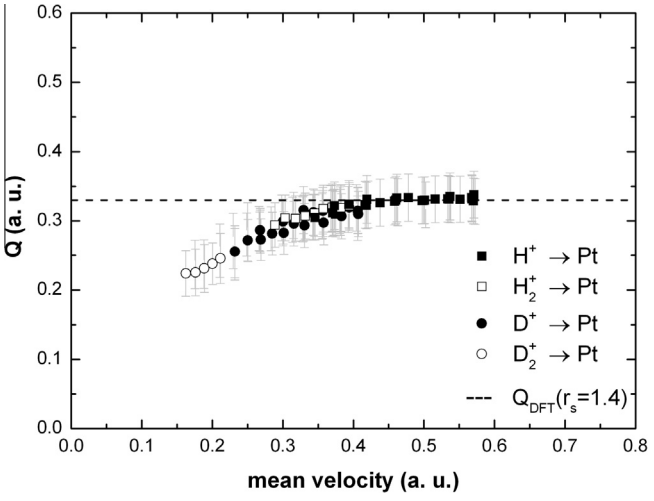

Fig. 9. Experimental values of the electronic friction coefficient Q for H^+, D^+ and D_2^+ fragments in Pt. The dashed line shows the Q values calculated according to the DFT for $r_s = 1.4$.

6. Discussion

The most interesting aspect of these measurements are the new evidences on the deviations from the proportionality with ion speed. This effect is at variance with the predictions of the free electron gas models, including linear and non-linear (DFT) calculations. As described in the Introduction, similar effects have been reported earlier by Valdés et al. [12,13] for some metals containing d electrons, such as Cu, Ag, and Au, and attributed to the particular characteristics of the d electrons of those metals. However, recent measurements on Pd foils [18] did not show such effects. The striking difference between Pd and Pt is therefore a point of great interest and requires more specific theoretical analysis.

To illustrate some differences in the electronic properties of these two elements, we show in Fig. 10 the density of states (DOS) of Pd and Pt, calculated using the TB-LMTO methods [41]. The lines in this figure show the different components (s, p and d bands) as well as the total DOS. The high-energy edge of the distribution is in both cases a little above the Fermi level. We notice a larger accumulation of the energy levels of Pd close to this level as compared with Pt. Another significant difference that we may observe is the wider spread of the DOS of Pt as compared with Pd. The intriguing question here is weather these differences in the DOS could be enough to explain the differences in the behavior of the corresponding energy losses.

A simplified model to incorporate the influence of the DOS on the low-energy stopping power has been proposed in previous works [42,43]. The model takes into account the electronic properties of the transition metals, expressed by the corresponding density of states (DOS). In this model the mean energy loss of a low-energy ion moving in a metal is represented in terms of the transport cross section (TCS), which is calculated using the partial wave and phase-shift formulations of quantum scattering theory, as described in the previous references. The stopping power is obtained as an integral of the energy transfer cross section over the DOS of the target using the relation $\langle \frac{dE}{dx} \rangle = vQ(v)$, where the velocity dependent friction coefficient $Q(v)$ is given by

$$Q(v) = v_F^{(s,p)} \int_0^{\epsilon_F} \sigma_{tr}^{(s,p)} n_{sp} d\epsilon + v_F^{(d)} \int_0^{\epsilon_F} \sigma_{tr}^{(d)} n_d d\epsilon \qquad (5)$$

where n_{sp} and n_d represent the density of states of the sp and d electron bands, and $\sigma_{tr}^{(s,p)}$ and $\sigma_{tr}^{(d)}$ are the corresponding transport cross sections for the excitation of those electrons, calculated as described in [42,43].

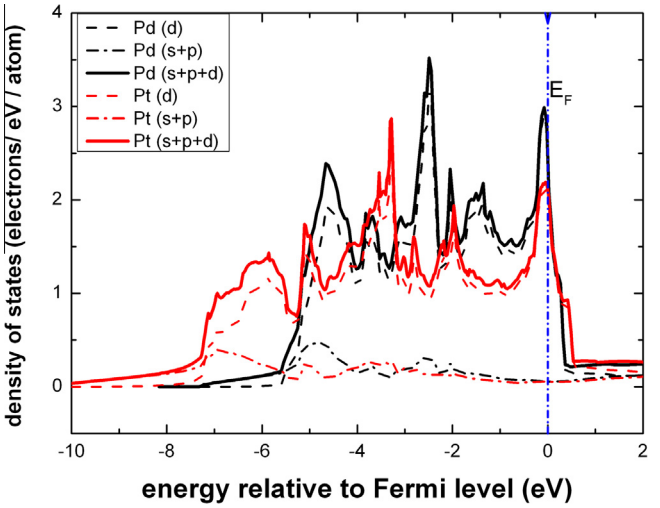

Fig. 10. Density of states of Pt and Pd, including the contributions of s, p, and d electrons.

The calculation according to Eq. (5) using the TCS approach [43] and the DOS of Pt is shown in Fig. 8. For a better test of the velocity dependence, the theoretical curve was normalized to the mean value of the highest energy data points since at that energy a straight line behavior is obtained. The absolute theoretical results were also included in this figure (black solid line) in order to show that the agreement with respect to the experimental results is very good, less than 5% for the larger discrepancy. The normalized theoretical curve (line with stars) was plotted to discuss the mean velocity dependence. As it may be observed, the theoretical model yields an excellent description of the observed bending of the experimental results on the whole range of low velocities. The physical explanation of this effect comes from the way the projectile excites the *d* electrons. At very low projectile energies the energy loss is due to the excitation of electrons with energies close to the Fermi level; with increasing ion energies more electrons in the DOS distribution are incorporated to the energy loss process and the stopping curve gradually approaches the velocity proportionality predicted by the DFT, with an effective r_s value corresponding to the excitation of all the *s*, *p*, and *d* electrons. This condition is reached at higher projectile velocities for wider DOS distributions. As shown in Fig. 8, this condition is reached for (still low) ion velocities $v \sim 0.4$—0.6 atomic units.

The explanation given here works very well in the case of Pt, but there seems to be a contradiction with the velocity dependence reported before for Pd in the same energy range [18], since the DOS of both metals show similar DOS structures (Fig. 10), and moreover, they belong to the same Group 10 in the Periodic Table. In order to explain this seeming contradiction we decided to apply the same theoretical model to Pd. The results are shown in Fig. 11. In this figure we show the experimental data from Ref. [18] together with the results of the present TCS-DOS model calculated with Eq. (5) using the DOS of Pd. The other two straight lines show the results of the DFT and an alternative model calculation using the Extended Friedel Sum Rule from Ref. [44], which both predict a linear v dependence. An interesting result shown in this figure is that in the case of Pd the present model shows a much smaller deviation from the velocity proportionality with respect to the DFT prediction, while the experimental results for $v > 0.15$ a.u. do not show such deviations. We notice, however, that the effect obtained with this model, in the case of Pd, is so small that it could have not been detected in the energy range covered by the previous experiments. A more detailed numerical study shows that the wider spread in energies of the DOS of Pt, together with its lower accumulation of states near the Fermi level are the main features that produce the different velocity dependences. It may also be noted that the typical energy transfer in binary collisions between an ion with speed v and a target electron with speed v_e, in the low energy range ($v < v_e$), is given by $\sim m\, v\, v_e$. Thus, considering proton or deuteron velocities between 0.15 and 0.3 atomic units, we obtain typical values of energy transfers for these cases of the order of 5–11 eV, which may be compared with the widths of the DOS distributions for these two metals.

Therefore, the differences in the velocity dependences observed in Pd and Pt can be explained in a satisfactory way by the proposed model considering the properties of the DOS of both metals.

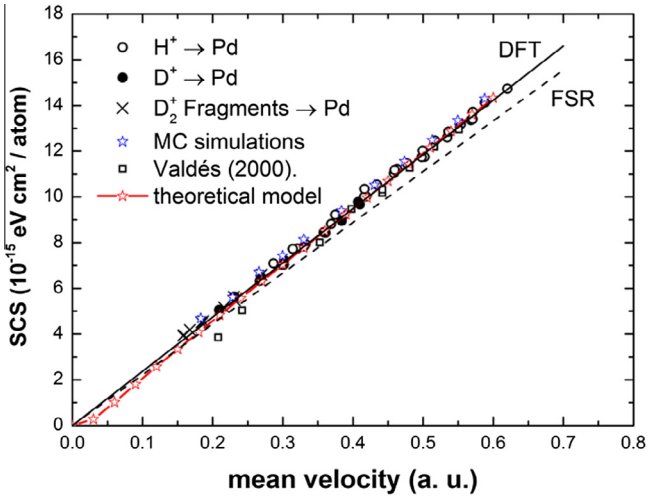

Fig. 11. Stopping cross section for hydrogen ions in Pd, as a function of the mean projectile velocity. The circles and squares show the experimental values; the blue stars are the MC simulations; the red-star line shows the result of the theoretical model of Eq. (5). (For interpretation of the references to color in this figure legend, the reader is referred to the web version of this article.)

7. Conclusions

Using the transmission technique we have determined the energy and angular distributions of light ions in polycrystalline Pt foils in the low energy range of 600 eV–10 keV. With this technique we have determined the angular dependence, the multiple scattering function, and the velocity dependence of the electronic energy loss of H^+, D^+, and D_2^+ fragments.

We performed MC simulations as well as calculations using the multiple scattering formalism of Ref. [35] and find good agreements with the experimental angular distributions, using the Molière and ZBL potentials with screening lengths $a_M = 0.83 a_L$ and $a_{ZBL} = 0.63 a_L$.

The analysis of the experimental results of the angular dependence of the energy loss using the three-components model [38] provides a useful method to determine the value of the surface roughness of the sample and to separate the effects of path-length enlargement, elastic energy loss and surface roughness. This method yields also a good agreement with the MC simulations.

The elastic energy loss contribution was independently extracted from MC simulations. For the conditions of our experiments, i.e. in transmission measurements with small angles of dispersion, this contribution is always very small. For the lowest-energy measurements in forward direction we obtain an elastic contribution of *ca.* 4%, which is too small to affect the velocity dependence of the forward energy loss.

The measurements of the electronic energy loss in the forward direction show a clear deviation from the velocity proportionality predicted by the DFT and other free-electron gas models, producing a significant deviation at low energies, $v < 0.4$ a.u, similar to the behavior observed in other transition metals (Cu, Ag, Au), and different from the case of Pd. The presence of "threshold effects" in Pt, may be explained by the distribution (DOS) of the *d*-electron bands in these metals. The present model, that includes the effects of the electronic distribution of the solid, reproduces very well the different behavior observed in Pd and Pt.

In summary, these new measurements provide information that contributes to improve the knowledge on the role of the *d* electrons in the phenomenon of the energy loss of light ions in transition metals in the range of very low energies.

Acknowledgments

This work was partially supported by ANPCYT, Argentina (PICT 124-2012), the Universidad Nacional de Cuyo (06/C440), and CONICET, Argentina (PIP 112 201101 00594). We acknowledge help with film growth by Mr. I. Artola Vinciguerra, and XPS measurements performed by G. Zampieri. Useful comments by P. Grande are gratefully acknowledged.

References

[1] F. Lazara, A. Morina, N. Paucb, P. Gentileb, S. Donetc, L. Guetaza, O. Sicardya, Electrochim. Acta 78 (2012) 98–108.
[2] J. Xie, S. Wang, L. Aryasomayajula, V.K. Varadan, Nanotechnology 18 (2007) 065503.
[3] G. Zhang, S. Sun, M. Cai, Y. Zhang, R. Li, X. Sun, Sci. Rep. 3 (2013) 1526.
[4] N.W. Pu, C.A. Wang, Y.M. Liu, D.Y. Liu, P.C. Wang, M.D. Ge, J. Nanosci. Nanotechnol. 13 (2013) 5702.
[5] V.B. Jadhava, Y.J. Juna, J.H. Songa, M.K. Parka, J.H. Ohb, S.W. Chaeb, I.-S. Kimc, S.-J. Choic, H.J. Leeb, Y.S. Sohna, J. Control Release 147 (2010) 144.
[6] E. Porcel, S. Liehn, H. Remita, N. Usami, K. Kobayashi, Y. Furusawa, C. Le Sech, S. Lacombe, Nanotechnology 21 (2010) 085103.
[7] J. Lindhard, K. Dan, Vidensk. Selsk. Mat. Fys. Medd. 28 (8) (1954) 1.
[8] T.L. Ferrell, R.H. Ritchie, Phys. Rev. B 16 (1977) 115.
[9] P.M. Echenique, R.M. Nieminen, R.H. Ritchie, Solid State Commun. 37 (1981) 779.
[10] A. Mann, W. Brandt, Phys. Rev. B 24 (1981) 4999.
[11] M.J. Puska, R.M. Nieminen, Phys. Rev. B 27 (1983) 6121.
[12] J.E. Valdés, G. Martínez Tamayo, G.H. Lantschner, J.C. Eckardt, N.R. Arista, Nucl. Instrum. Meth. B 73 (1993) 313.
[13] J.E. Valdés, J.C. Eckardt, G.H. Lantschner, N.R. Arista, Phys. Rev. A 49 (1994) 1083.
[14] E.D. Cantero, G.H. Lantschner, J.C. Eckardt, N.R. Arista, Phys. Rev. A 80 (2009) 032904.
[15] S.N. Markin, D. Primetzhofer, S. Prusa, M. Brunmayr, G. Kowarik, F. Aumayr, P. Bauer, Phys. Rev. B 78 (2008) 195122.
[16] S.N. Markin, D. Primetzhofer, M. Spitz, P. Bauer, Phys. Rev. B 80 (2009) 205105.
[17] M.A. Zeb, J. Kohanoff, D. Sanchez-Portal, A. Arnau, J.I. Juaristi, E. Artacho, Phys. Rev. Lett. 108 (2012) 225504.
[18] C. Celedón, E.A. Sánchez, M.S. Moreno, N.R. Arista, J.D. Uribe, M. Mery, J.E. Valdés, P. Vargas, Phys. Rev. A 88 (2013) 012903.
[19] D. Isaacson, Compilation of rs values, Internal Report, Rad. and Sol. State Lab., NY University, 1975.
[20] D. Goebl, D. Roth, P. Bauer, Phys. Rev. A 87 (2013) 062903.
[21] D. Primetzhofer, Phys. Rev. B 86 (2012) 094102.
[22] Colutron Research Corporation, Boulder, Colorado, USA, <http://www.colutron.com>.
[23] <http://anales.fisica.org.ar/journal/index.php/analesafa/article/view/885/954>.
[24] R.S. Bhattacharya, W. Eckstein, H. Verbeek, Surf. Sci. 93 (1980) 563–581.
[25] R.A. Vidal, F. Bonetto, J. Ferrón, M.A. Romero, E.A. García, E.C. Goldberg, Surf. Sci. 605 (2011) 18–23.
[26] L.N. Serkovic Loli (PhD thesis), Instituto Balseiro, Universidad Nacional de Cuyo, 2010. <http://ricabib.cab.cnea.gov.ar/153/1/1Serkovic.pdf>.
[27] E.A. Figueroa, N.R. Arista, J.C. Eckardt, G.H. Lantschner, Nucl. Instrum. Meth. B 256 (2007) 126.
[28] M. Bjorck, G. Andersson, J. Appl. Crystallogr. 40 (2007) 1174.
[29] L.G. Parratt, Phys. Rev. 95 (1954) 359.
[30] E. Chason, T.M. Mayer, Crit. Rev. Solid State Mater. Sci. 22 (1997) 1–67.
[31] B.L. Henke, E.M. Gullikson, J.C. Davis, X-ray interactions: photoabsorption, scattering, transmission, and reflection at E = 50–30,000 eV, Z = 1–92, Atomic Data Nucl. Data Tables 54 (1993) 181–342. <http://www-cxro.lbl.gov/>.
[32] J.F. Ziegler, J.P. Biersack, SRIM-2010 – the stopping and range of ions in matter, code available in <http://www.srim.org>.
[33] W. Möller, G. Pospiech, G. Schrieder, Nucl. Instrum. Meth. 130 (1975) 265.
[34] M. Famá, J.C. Eckardt, G.H. Lantschner, N.R. Arista, Phys. Rev. A 62 (2000) 062901.
[35] P. Sigmund, K.B. Winterbon, Nucl. Instrum. Meth. 119 (1974) 541.
[36] W. Eckstein, Computer Simulation of Ion-Solid Interactions, Springer-Verlag, Berlin, 1991.
[37] M. Nastasi, J.W. Mayer, J.K. Hirvonen, Ion-Solid Interactions, Cambridge University Press, 1996.
[38] M. Famá, G.H. Lantschner, J.C. Eckardt, C.D. Denton, N.R. Arista, Nucl. Instrum. Meth. B 241 (2000) 164.
[39] E.D. Cantero, G.H. Lantschner, J.C. Eckardt, F.C. Lovey, N.R. Arista, Phys. Rev. A 81 (2010) 042902.
[40] E.D. Cantero, G.H. Lantschner, N.R. Arista, Eur. Phys. J. D 65 (2011) 397.
[41] O.K. Andersen, O. Jepsen, Phys. Rev. Lett. 53 (1984) 2571.
[42] J.E. Valdés, P. Vargas, N.R. Arista, Phys. Rev. A 56 (1997) 4781.
[43] E.A. Figueroa, E.D. Cantero, J.C. Eckardt, G.H. Lantschner, J.E. Valdés, N.R. Arista, Phys. Rev. A 75 (2007) 010901.
[44] A.F. Lifschitz, N.R. Arista, Phys. Rev. A 57 (1998) 200.